ORIGINAL ARTICLE

lajss.org© Latin American Journal of Solids and Structures

www.lajss.org

Interference effects mapping on the static wind loading of a tall building

Thiarly Feitosa Afonso de Lavôr[a]* , José Luis Vital de Brito[a] , Acir Mércio Loredo-Souza[b]

[a] Universidade de Brasília, PECC, SG-12, 70910-900, Brasília, DF, Brasil. E-mail: thiarlycz@hotmail.com, jlbrito@unb.br
[b] Universidade Federal do Rio Grande do Sul, LAC, 91501-970, Porto Alegre, RS, Brasil. E-mail: acir@ufrgs.br

* Corresponding author

https://doi.org/10.1590/1679-78257330

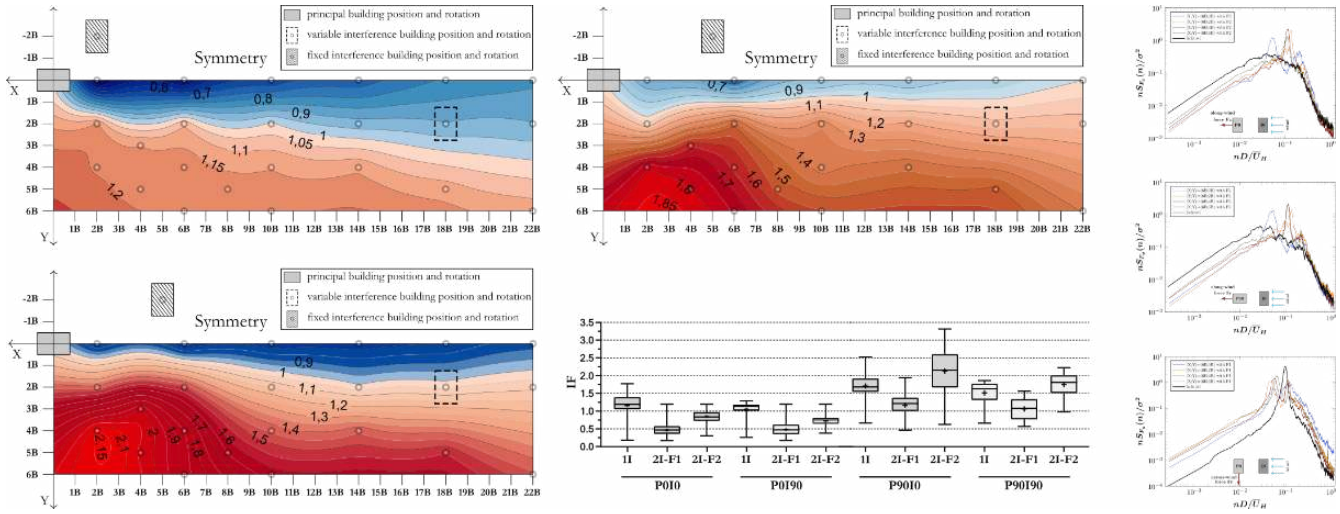
Abstract

Wind-induced loading on buildings may be altered due to presence of upwind structures. These variations are quantified by the interference factors (IFs), which is determined experimentally for each case analyzed, since obtaining this quantification in codes and standards is still impractical due to the complexity of the multi-parameters involved. To understand the influence of some of these parameters on the interference effects, contour plots and power spectra density were presented for IFs corresponding to aerodynamic coefficients of the along-wind and cross-wind force, as well as for torsion. Wind tunnel tests were conducted applying the synchronous pressure measurement technique. Interference arrangements with one and two upstream interfering buildings were investigated for different wind angles, relative positions and terrain roughness. Results indicate that the shielding effect is predominant in most of the studied cases. Nevertheless, the amplification effects are generally present in specific configurations and are usually caused by channeling and buffeting effects, as well as vortex shedding.

Keywords

Tall buildings; Interference effects; Along-wind; Across-wind; Torsion; Wind tunnel

Graphical Abstract



Received: October 12, 2022. In revised form: February 07, 2023. Accepted: March 20, 2023. Available online: March 24, 2023.
https://doi.org/10.1590/1679-78257330

Latin American Journal of Solids and Structures. ISSN 1679-7825. Copyright © 2023. This is an Open Access article distributed under the terms of the Creative Commons Attribution License, which permits unrestricted use, distribution, and reproduction in any medium, provided the original work is properly cited.

1 INTRODUCTION

With the increase in the building's height, wind loads became a determining factor in the structural analysis design. One of the wind effects that is considered in structural designs is the interference effects due to surrounding buildings. Some researchers in the past have also investigated and indicated the importance of the interference effect, analyzing parameters such as the number of interfering buildings and its locations, simulated wind characteristics and its angle of incidence, terrain roughness, relative dimensions of buildings, modal frequency, mode shapes, Scruton number and Strouhal number (Gu et al. (2005), Vieira et al. (2018), Lo et al. (2020), Fontes-Silva et al. (2022)).

Due to the complexity of the phenomenon, involving multi-parameter, some standards and design codes recommend wind tunnel tests to obtain the interference effects while some others have numerical indications of this effects in its scope (IS 875 (2015), ABNT NBR 6123 (1988)). Most references deal with interference effects based on their influence on the mean and fluctuating components of loads (pressure/force, bending and torsional moments) and responses (acceleration and displacement) on tall buildings, obtained by applying the high frequency force balances or by pressure measurement techniques, which allows an investigation of the change on local wind load, in addition to the overall wind design loads.

In Mara et al. (2014) a general reduction was observed in the mean and RMS along-wind moments. Meanwhile there was amplification in the across-wind RMS responses when the upstream buildings are in tandem positions in open terrain. Interference factors above 1.4 for RMS across-wind responses and above 1.5 for RMS torsion were obtained in oblique positions. These values decrease significantly in rougher terrain. Kim et al. (2015) observed interference factors peaks above 1.35 in the mean along-wind moment coefficients. The RMS interference factors with maximum values were obtained when the interfering building was located in the X/B = 1.5 and Y/B = 1 coordinates, B being the width of the building. It was verified by Yu et al. (2016) that the interference factor peak, without vortex shedding resonance, was 1.9 and 2.98 with the resonant effect on the torsional response.

Through few published studies on interference effects in unusually shaped buildings, it was found that this parameter has significant influence on interference effects. To quantify this influence, local pressure distribution was investigated by Pal et al. (2021a, 2021b), finding maximum suctions in a triangular model 40% higher than in square models and moments in the cross-wind direction dominating the overall model behavior due to its unsymmetrical cross-sectional shape.

In this paper, a series of wind tunnel tests were carried out to analyze interference effects (IEs) on wind loads resisted by a tall building (CAARC Standard Building), due to one and two upstream buildings. For this, the high frequency pressure integration (HFPI) method, which is based on synchronous pressure measurement technique, was used to obtain wind-induced statics loading. The IEs on along-wind and across-wind total force coefficient, as well as on torsion, were quantified by interference factors (IFs) and represented in contour plots, covering all upstream building positions. Furthermore, power spectral density (PSD) was used to characterize the analyzed parameters influence on the underlying aerodynamic phenomenon.

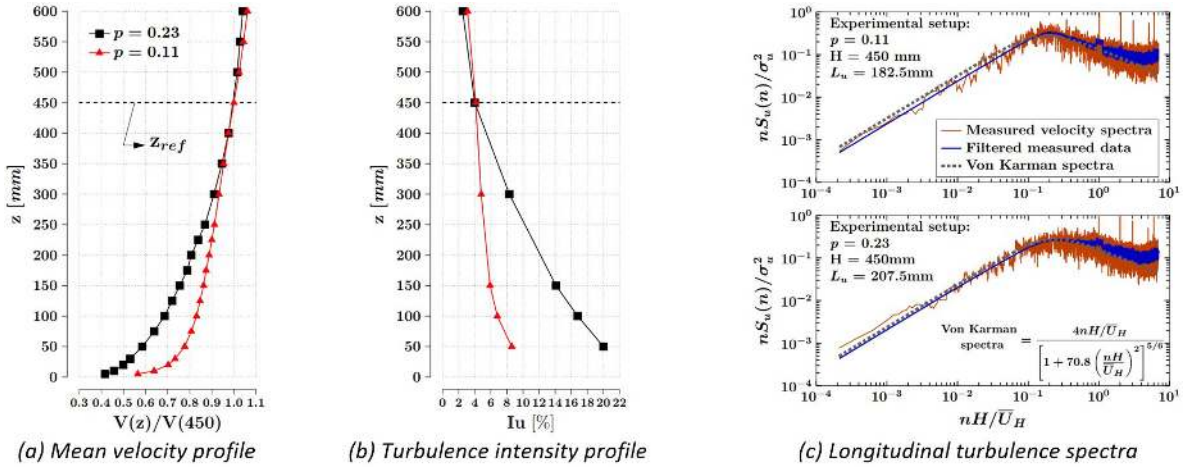
2 EXPERIMENTAL SETUP

2.1 Wind Tunnel

The tests were carried out at the Buildings Aerodynamics Laboratory of the Universidade Federal do Rio Grande do Sul (LAC-UFRGS), Brazil, using the Joaquim Blessmann Boundary Layer Wind Tunnel. It is a boundary layer wind tunnel and its test section, used in this study, is 1300 mm in width, 900 mm in height and 9320 mm in length. Two types of wind flow were simulated, where the mean wind velocity profile follows the power-law exponents equal to 0.11 and 0.23, correspond, respectively, to Category I and between Categories II and III of the Brazilian Wind-Load Code, NBR 6123 (1988). The flow characteristics along the height are represented in Figure 1 by the mean velocity profile, the turbulence intensity profile and the normalized along-wind turbulence spectra, which is a function of the frequency, n, reduced by the height of the measurement point, H, and the mean velocity at that point, $\overline{U}_H$.

The HFPI method is a practical and accurate option to measure wind pressures on an instrumented building model and then estimate static and dynamic responses of its prototype structural system. As a useful feature of the method, the aerodynamic force, bending and torsional moments are obtained along the height of the structure, and not only at the base (in case of force balances), providing more precision in the wind loading calculation, as well as allowing for the multiple mode shapes. The method limitation lies in the model shape, which must be rigid, therefore there is no possibility of capturing the fluid-structure interaction effects.

The pressures must be measured simultaneously in a large number of points on the model surface at a sample rate high enough so that its spectral density covers the first natural frequencies of vibration of flexible structural systems, usually in the range from 0.1 to 1Hz. Thus, an electronic pressure scanning module made by Scanivalve Corp, model ZOC33, with 64 channel pressure inputs for each module, with a maximum sample rate of 20kHz and an inaccuracy of 0.12%, was used. For the tests, 6 modules recorded n_P = 8192 pressure measurements per channel, in a sampling period of T = 16s, therefore the sampling frequency for the pressure data was 512Hz.

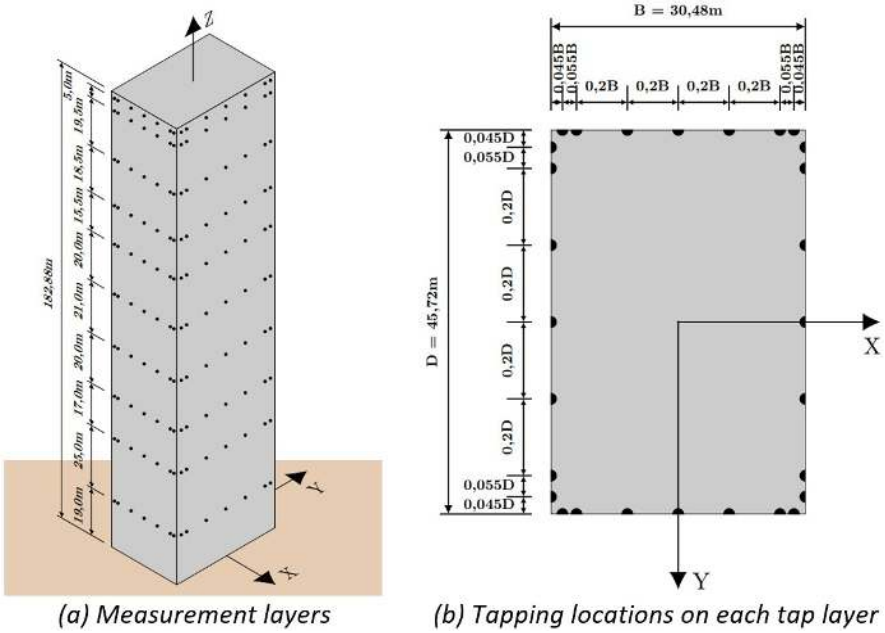


(a) Mean velocity profile (b) Turbulence intensity profile (c) Longitudinal turbulence spectra

Figure 1 Simulated wind parameters

The pressures must be measured simultaneously in a large number of points on the model surface at a sample rate high enough so that its spectral density covers the first natural frequencies of vibration of flexible structural systems, usually in the range from 0.1 to 1Hz. Thus, an electronic pressure scanning module made by Scanivalve Corp, model ZOC33, with 64 channel pressure inputs for each module, with a maximum sample rate of 20kHz and an inaccuracy of 0.12%, was used. For the tests, 6 modules recorded n_P = 8192 pressure measurements per channel, in a sampling period of T = 16s, therefore the sampling frequency for the pressure data was 512Hz.

These modules were connected to the building model through measuring tubes. The model was made of acrylic, 450mm in height and 112.5mm x 75mm in the plan, with a length scale of 1:406.4. The pressure taps were distributed along the perimeter of the model in 10 levels, each containing 28 points (7 per facade), totaling N = 280 pressure taps, arranged as shown in Figure 2, with full-scale dimensions.



(a) Measurement layers (b) Tapping locations on each tap layer

Figure 2 Principal building dimensions

2.2 Interfering Buildings Arrangement

The interference effects were analyzed according to the position and number of interfering buildings, with the same dimension as the instrumented model identified here as principal building. The grid arrangement of different relative positions of the interfering buildings, Figure 3, can be classified into three experiment sets: 1) 1 interfering building varying its position by 23 points (1I); 2) 2 interfering buildings, one varying its position by 23 points and the other fixed at point 1 (2I-F1); 3) 2 interfering buildings, one varying its position by 23 points and the other fixed at point 2 (2I-F2).

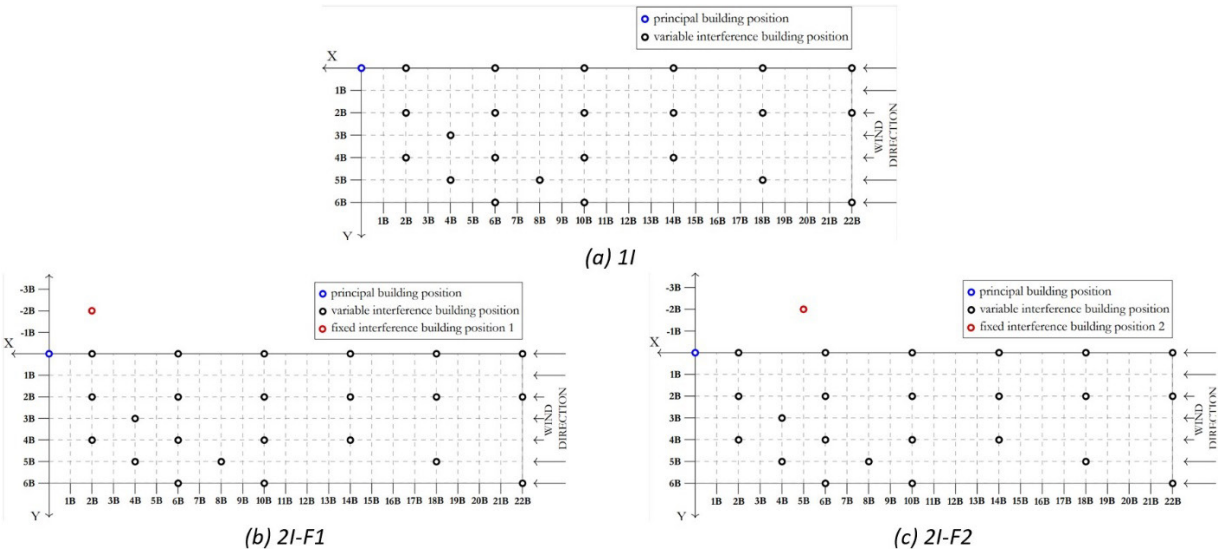


Figure 3 Coordinate grid of interfering buildings position

Where B is the smaller plan dimension of the principal building and the X-axis is the wind tunnel centerline. All interfering buildings cases, without pressure taps, were to the windward of the principal building. Their coordinates positions were chosen in order to evaluate the distance in tandem and staggered positions, in addition to the combined effect when the principal building is located at the edge of the wake shed by the fixed interference building. These positions are indicated on the grid by small circles and refer to building geometric center.

Assigning the angles of 0° and 90° to all buildings when, respectively, its longer and smaller plan side are perpendicular for wind incidence, Figure 4. Obviously, other wind incidence angles are important in the analysis of IEs, however here it was limited to those mentioned.

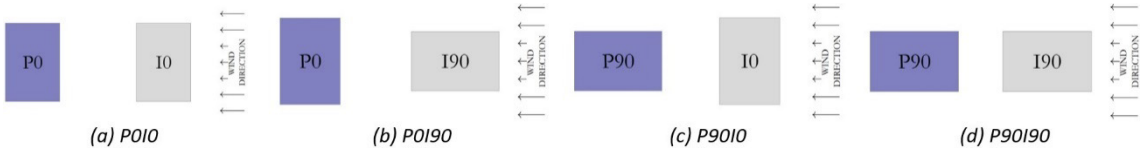


Figure 4 Relative rotations of buildings

Relative rotations sets were carried out between the principal building and the interfering one, against the wind incidence: 1) Principal and Interference buildings at 0° - P0I0; 2) Principal building at 0° and Interference building at 90° - P0I90; 3) Principal building at 90° and Interference building at 0° - P90I0; 4) Principal and Interference buildings at 90° - P90I90. The fixed interfering building, when present, follows the same rotation as the variable interfering building.

2.3 Data Analysis

The most convenient and common way to analyze the time series of wind pressures is through aerodynamic coefficients, which were calculated as follows:

$$C_F(t) = \frac{F(t)}{q \cdot B \cdot H} \tag{1}$$

$$C_T(t) = \frac{T(t)}{q \cdot B \cdot D \cdot H} \tag{2}$$

Where $C_F(t)$ and $C_T(t)$ are, respectively, instantaneous total force and torsional moment coefficients; $F(t)$ and $T(t)$ are, respectively, instantaneous total force and torque; B, D and H are, respectively, the smaller plan side, longer plan side and height of the studied building; q is the dynamic pressure, measured at the building model height.

The total force of the wind, acting on a building surface at a certain time, can be determined as follows:

$$\vec{F}(t) = \int_S P(t) \cdot \vec{\theta} \cdot dA \tag{3}$$

Where $\vec{F}(t)$ is the vector of the instantaneous total force; $P(t)$ is the pressure at the time t, integrated to the area A of the surface S, where the total force must be obtained and $\vec{\theta}$ is the direction cosine of the normal to that surface.

In HFPI, the number of pressure taps is finite and each one is associated with a tributary area. It is admitted that the vector pressure is always perpendicular to its tributary area, when it has positive value, it will have inside direction to pressure tap and when it has negative value, it will have outside direction to pressure tap and will mean suction.

The overall wind load acting on the building model, throughout the measurement period, can be represented simply by its components on the reference axes, as follows:

$$F_{x,\alpha} = F_{facade1,\alpha} + (-F_{facade3,\alpha}) \tag{4}$$

$$F_{y,\alpha} = F_{facade2,\alpha} + (-F_{facade4,\alpha}) \tag{5}$$

Where $F_{x,\alpha}$ and $F_{y,\alpha}$ are the components of the overall wind load, with incidence angle α (0° or 90°). Each component is the sum of the forces on the facades parallel to each other, according to Figure 5a. The negative sign in the forces of facades 3 and 4 occurs for the pressure and suction to be compatible with the directions of the reference axes. The overall wind load on the analyzed facade is calculated according to the following equation:

$$F_{facade,\alpha} \cong \sum_{j=1}^{n_P} \sum_{i=1}^{n_f} P_{i,j,\alpha} \cdot A_i \tag{6}$$

n_P is the total number of pressure measurements and n_f is the number of pressure taps on the considered facade. Considering the pressure tap i, A_i is its tributary area and $P_{i,j,\alpha}$ is the instantaneous pressure. The tributary areas were delimited according to Figure 5b, being d the distance between adjacent pressure taps.

Considering the building surface perimeter, the torsion moment can be written acting around its geometric center as follows:

$$M_{T,\alpha} \cong \sum_{j=1}^{n_P} \sum_{i=1}^{n_S} P_{i,j,\alpha} \cdot A_i \cdot l_i \tag{7}$$

Where n_S is the total number of pressure taps on the model surface and l_i is the distance between the actuation line projection of the measurement point and the center of torsion of the building, as shown in Figure 5a.

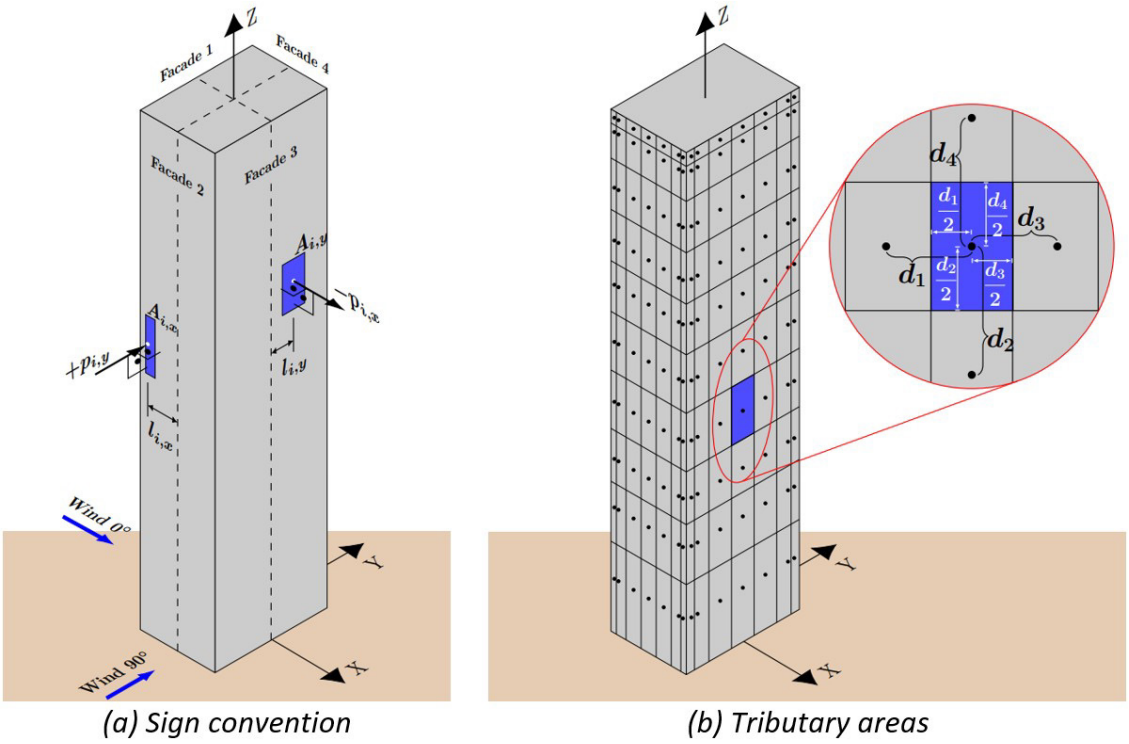


Figure 5 Pressure measurement on building model

There were some test cases in the presence of two interfering buildings with a blockage factor larger than 10%, these cases had their dynamic pressure values corrected. According to Barlow et al. (1999) this correction can be determined as follows:

$$q_b = q\left(1 + \frac{1}{4}\frac{A_b}{A_t}\right)^2 \tag{8}$$

Where q_b is the dynamic pressure corrected by the blockage; the blockage area, A_b, is the sum of the effective frontal areas of the models ("shadow area"); and A_t is the wind tunnel test section area.

From the sampling time of the instantaneous aerodynamic coefficients, it was possible to determine their mean and RMS values. The Figure 6 show the time histories of the principal building in its isolated case.

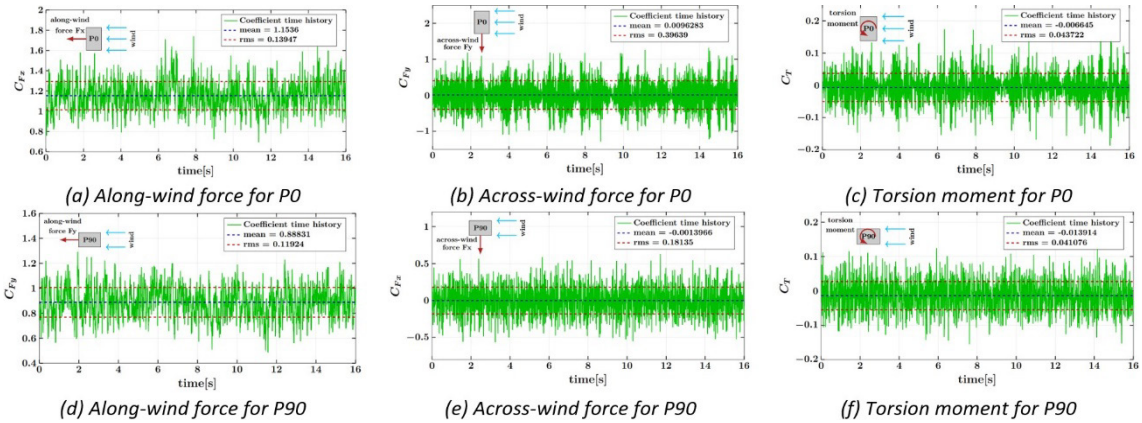


Figure 6 Time history of aerodynamic coefficients for isolated building

After determining the mean and RMS coefficients for all upstream building cases, the interference effects can be estimated. These effects are usually represented using the interference factor (IF), which indicates the change in the

wind load acting on a building, caused by upstream or downstream buildings. The IF is defined below, where C is the analyzed aerodynamic coefficient on the principal building.

$$IF = \frac{C \text{ in the presence of the interfering building}}{C \text{ in the isolated principal building case}} \tag{9}$$

3 RESULTS AND DISCUSSIONS

3.1 Interference Effects

With the interference factors (IFs) of the aerodynamic coefficients calculated from the experimental data, contour plots were plotted using the *Kriging* regression method. For simplicity, the results of negative Y-axis coordinates can be considered equivalent to the results shown on positive Y-axis when experimental cases of building arrangements are mirrored, and for that reason it was not plotted. The results of negative X-axis have different values from the positive X-axis and was not presented since there were no experimental results in these positions.

The contour plots axes are parallel and perpendicular to the incident wind, which makes it convenient to obtain and exhibit the IFs of the mean along-wind and RMS across-wind forces and RMS torsional moment. Due to the mean value of across-wind and torsional loads tending to zero in isolated model case, the use of RMS value becomes more appropriate. The contour plots presented here are only for the roughness p = 0.23, with the rotations of the buildings shown in Figure 4 and for the three interfering building sets, shown in Figure 3.

3.1.1 Along-wind Force

The contour plots with the principal building at 0° (P0), Figure 7, have an extensive area of protection (shielding effect) caused by the interfering building, mainly in the presence of 2 upstream buildings. The amplification effects are present in Y-axis coordinates from 1.5B and along the range of X-axis for the 1 upstream building cases, both in P0I0, Figure 7a, and in P0I90, Figure 7d, with amplification zone a little less extensive in this last configuration.

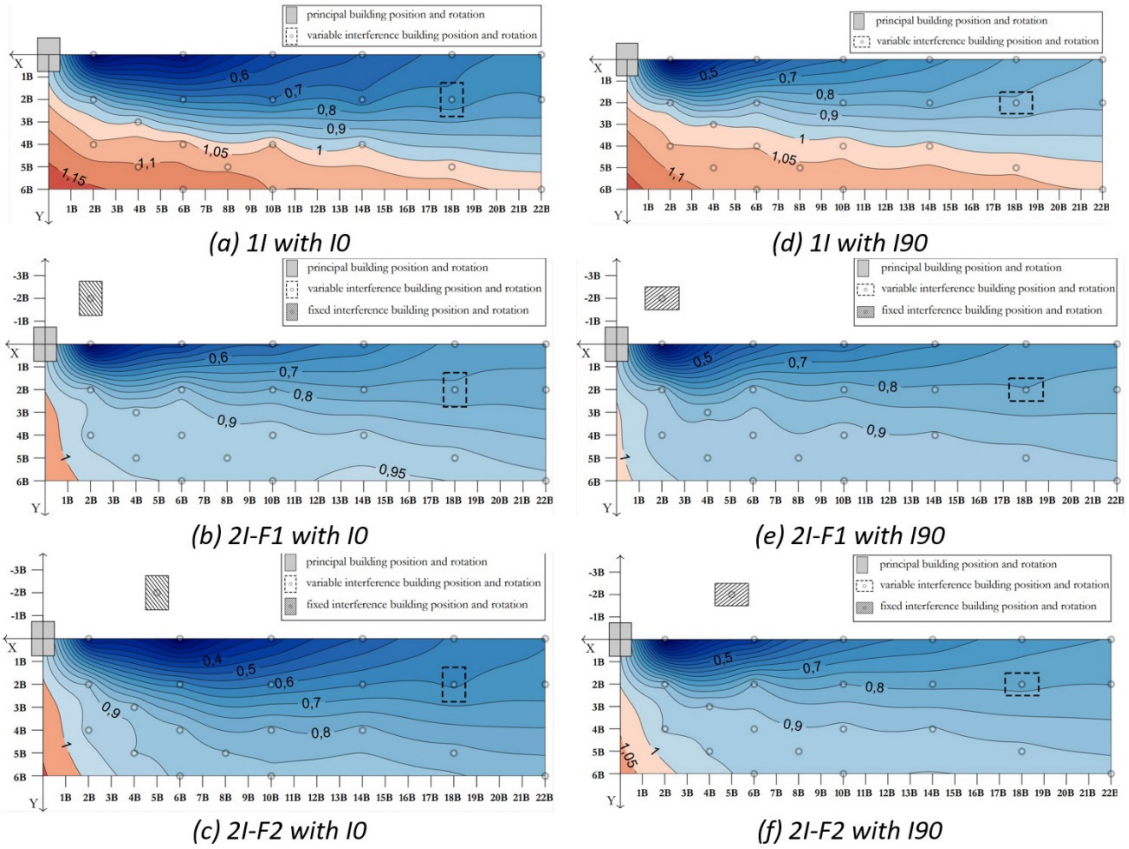


Figure 7 Contour plots of mean along-wind force coefficients IFs for P0

This signalizes the influence that the interfering building width, and consequently the dimension of its wake vortex turbulence, has on the interference effects as noted by Hui et al. (2013), where the IFs due to interfering building were slightly higher, when its larger facade was normal to the wind incidence, compared to the IFs obtained when the wind was normally against to the smaller upstream building facade.

According to Figure 8, the amplification area with the principal building at 90° (P90) increases in all three upstream building sets, observing values of IFs ≥ 1.15. This greater amplification can be explained by the low value of the mean along-wind force on the analyzed building, when it is isolated in this rotation, Figure 6d. Therefore, any disturbance of the approaching wind flow, caused by the presence of the interfering building, allows for the increasing this loading. This can be verified in configurations with interfering buildings at 90° (I90), Figures 8d to 8f, where its IFs values were lower than in the configurations with interfering buildings at 0° (I0), Figures 8a to 8c, since these affects more the approaching wind flow, either with the turbulence increasing or with the generation of larger wake vortex.

The IFs values in the presence of fixed interfering building in position 1, Figures 8b and 8e, were even higher than the configurations with only one interfering building, indicating a scenario with the most affected approaching flow.

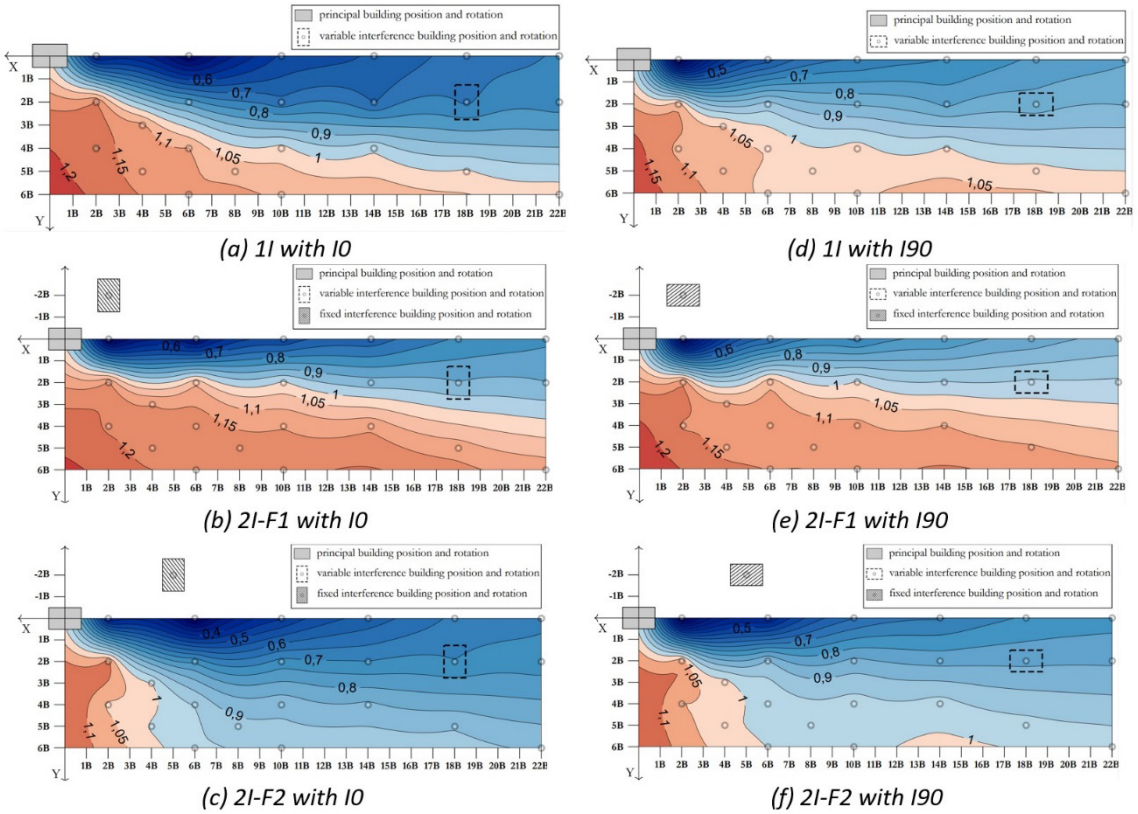


Figure 8 Contour plots of mean along-wind force coefficients IFs for P90

3.1.2 Across-wind Force

It can be seen from the contour plots with the principal building at 0° (P0), Figure 9, that the extension of shielding effect is high, mainly in configurations with the interfering building(s) at 90° (I90), Figures 9d to 9f. The amplification effects, on the other hand, are found with higher magnitude in configurations with interfering building(s) at 0° (I0), except in the presence of fixed interfering building in position 1, Figure 9b, which caused protection across the entire contour plot area. This behavior reinforces the understanding of a greater change in approaching wind flow due to the wake vortex, generated by the interfering building with its longer plan side perpendicular to the wind incidence.

Since the amplifications in across-wind fluctuations are caused, according to Taniike (1992), by the alternating vortex shedding, the contour plots results suggest the interruption of this effect in the presence of 2 interfering buildings. This attenuation reduces as the fixed interference building increases its distance from the principal building, especially at 0° (I0) rotation, where a wake vortex induced will achieve the principal building with a larger scale.

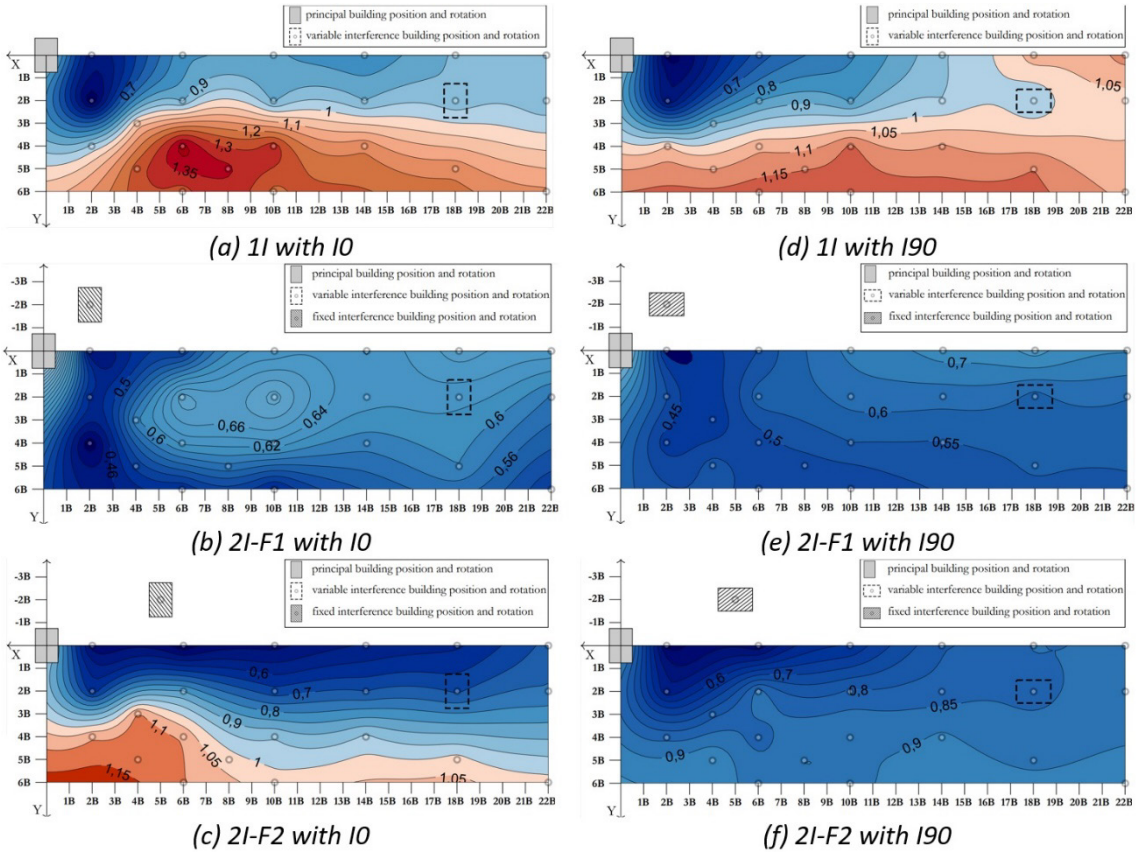


Figure 9 Contour plots of RMS across-wind force coefficients IFs for P0

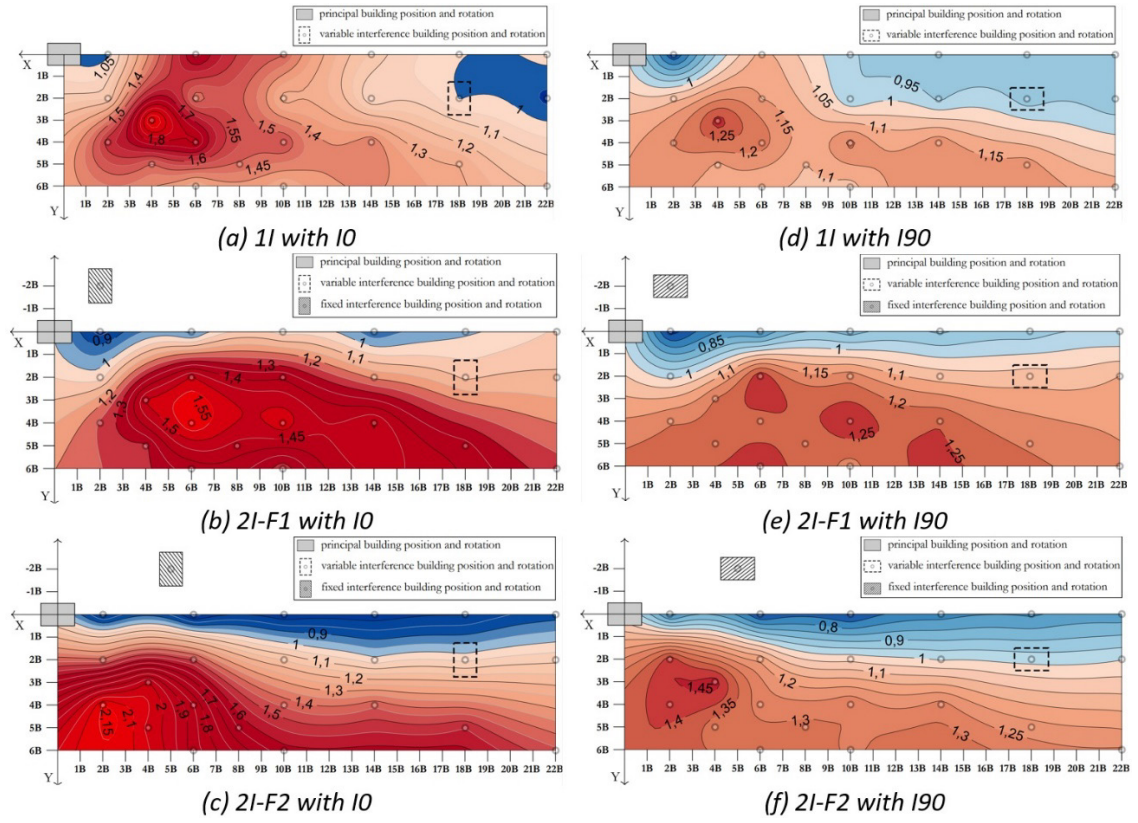


Figure 10 Contour plots of RMS across-wind force coefficients IFs for P90

The amplification area in contour plots with the principal building at 90° (P90), in all three upstream building sets, fills it nearly entirely and presents IFs from 1.55 to above 2.10 for interfering buildings at 0° (I0), Figures 10a to 10c, and IFs from 1.25 to above 1.45 for the upstream buildings at 90° (I90), Figures 10d to 10f. Similar results can be found in Mara et al. (2014) and Zu and Lam (2018), both in the IFs magnitude and in the critical values locations, despite the differences between the experimental setups of these researches. Again, it is noted that configurations with interfering building at 0° (I0) have higher amplification due to a likely more intense interference in the approaching wind flow, with the formation of larger wake vortex shedding.

It should be noted that all configurations with the principal building at 90° (P90) caused amplification in almost the entire contour plots extension, for both interfering buildings rotations. The maps showed shielding values only in the regions of alignment with the principal building (tandem positions), with a greater extent for interfering buildings at 90° (I90). This suggests that the across-wind loading is also very influenced by the change in approaching wind flow, caused by an upstream building with a smaller drag area.

3.1.3 Total Base Torsion Moment

The contours plots with the principal building at 0° (I0), Figure 11, showed a significant extension of shielding effect caused by the interfering building(s), especially in the presence of fixed interfering buildings. However, amplification effects are found for cases with only one upstream building, suggesting that the turbulence in approaching wind flow generated by the interfering building amplifies the fluctuations and the eccentricity of its overall force.

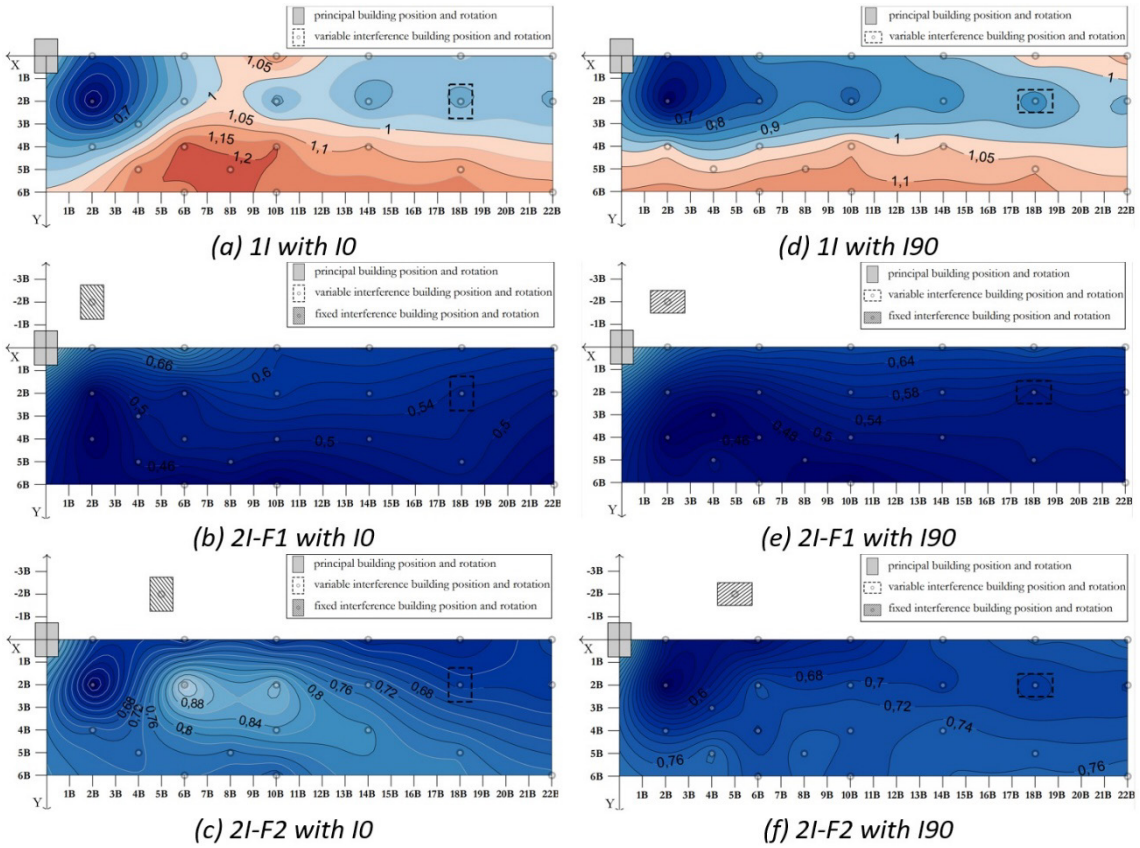


Figure 11 Contour plots of RMS torsion moment coefficients IFs for P0

As in previous analyses, the change in the interfering building rotation to the smaller plan side, normal to the wind incidence, caused a reduction in the amplification and increases the shielding zone extension. The distribution and magnitude of IFs values in contour plots presented here were similar to that analyzed by Zhang et al. (1994), where in general the IFs of the mean torsional moment, measured via an aeroelastic model, were lower in the presence of an interfering building with smaller cross-section. However, at an increasing of the neighbor width, passing a certain proportion, the effects are reversed, as seen in Hui et al. (2017), where the IFs of the torsional moment fluctuations, in the presence of an interfering building with its longer side perpendicular to the incident wind, were lower than the IFs for the case of wind against its short side, about one-third of the longer one. The amplification area with the principal

building at 90° (P90), Figure 12, fills the contour plots in almost its entirety, except in the presence of the fixed upstream building in position 1. These high values indicates that the torsional fluctuations has a significant sensitivity to the turbulence, generated by the upstream building(s), when the analyzed building has the smaller side normal to the wind incidence. Again, it is noted that the configurations with the interfering building(s) at 0° (I0) have greater amplification relative to the I90 sets.

Again, scenarios with the principal building at 90° (P90) had higher IFs than P0 configurations. This amplification in the fluctuations can be interpreted as an indication that situations at P90 are susceptible to resonant dynamic phenomenon, even in the presence of the second interfering building, especially when it is further away from the principal building.

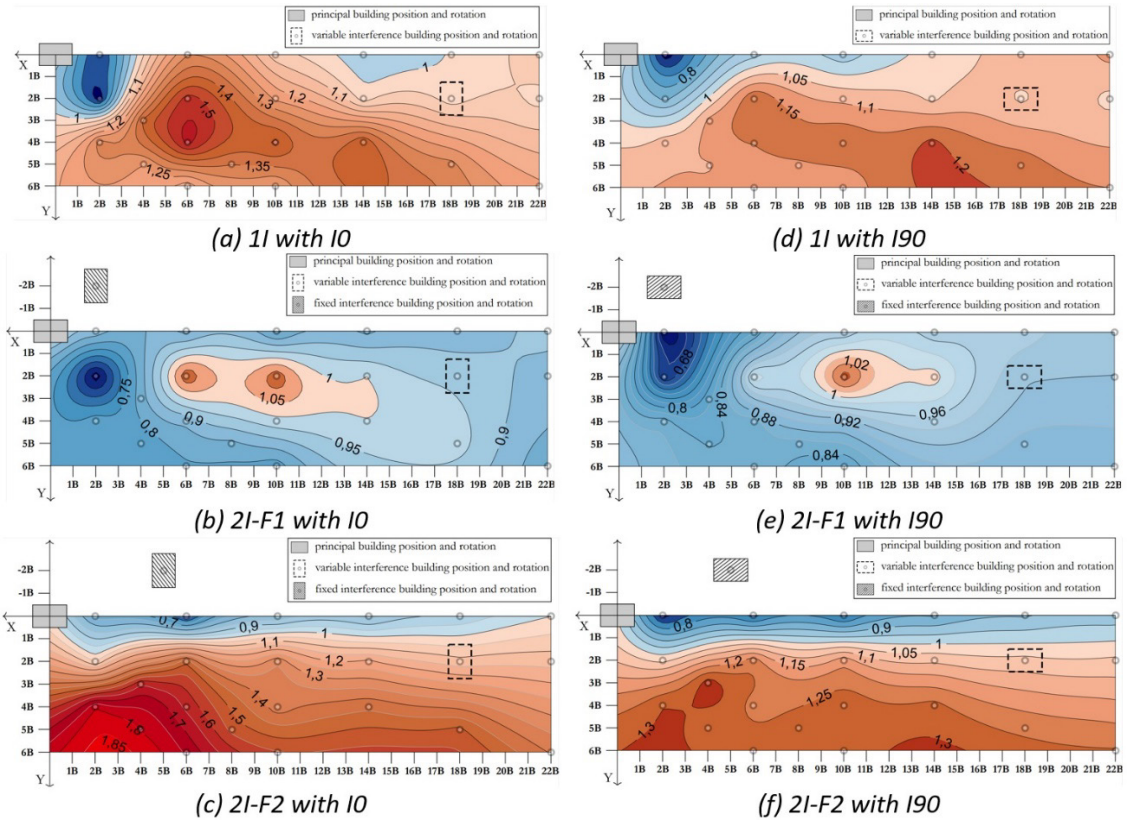


Figure 12 Contour plots of RMS torsion moment coefficients IFs for P90

3.2 Effects of Upstream Terrain

By the graphs in Figure 13a, a smaller variability can be observed with the principal building at 0° (P0I0 and P0I90) relative to its orientation at 90° (P90I0 and P90I90). It can be understood due to the higher level of shielding effect and the presence of few amplifications in the results with P0, when compared to P90 sets. By the graphs in Figure 13b, a similar variability between the roughness types was observed, nevertheless, with a slight tendency towards the superiority of the results with p = 0.23. It is possible to be affirmed that the IFs average value in the 2I-F1 sets is greater than unity, both for the P90I0 and P90I90 rotations, shown in Figure 13b. This roughness effect in the static analysis was also observed by Xie and Gu (2004) in situations with one and two interfering buildings, where the shielding effects were higher in the smoother terrain.

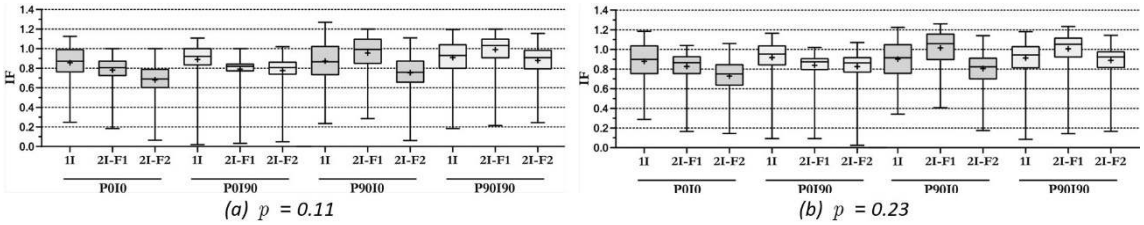


Figure 13 Variability of mean along-wind force coefficients IFs

As seen in the along-wind force, it is observed that the increases in turbulence intensity, due to the rougher terrain, amplified the across-wind force fluctuations, but not enough to cause non-similarity of the IFs with p = 0.11, Figure 14a, and with p = 0.23, Figure 14b. Both roughness terrain types presented important amplifications in configurations with the principal building at 90° (P90I0 and P90I90). The rougher terrain exhibited IFs with fewer variability, suggesting a minor influence of the interfering building location within the amplification zones.

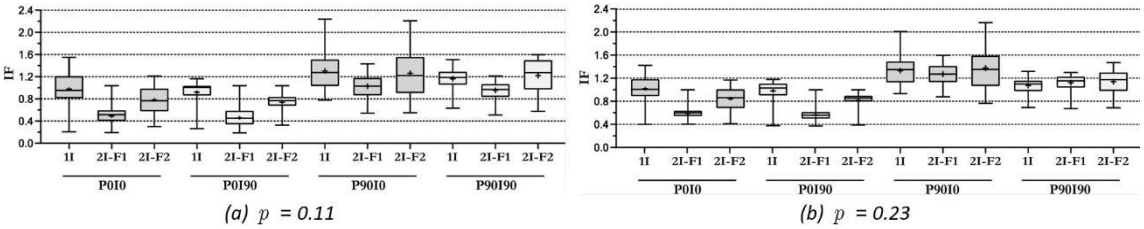


Figure 14 Variability of RMS across-wind force coefficients IFs

The graphs in Figure 15 show that, differently from the loads analyzed above, the torsional moment fluctuations were significantly influenced by the terrain roughness. The increase in turbulence, due to the increment in roughness, Figure 15b, caused a significant shielding effect and attenuation in amplifications. However, its IFs average values were above unity in configurations at P90 (P90I0 and P90I90), except in 2I-F1 upstream building sets. With p = 0.11, Figure 15a, there was much more significant amplifications relative to the rougher terrain, resulting in IFs average values above 1 in all of the upstream building cases at P90I0 and P90I90 and in the presence of one interfering building (1I) at P0I0 and P0I90.

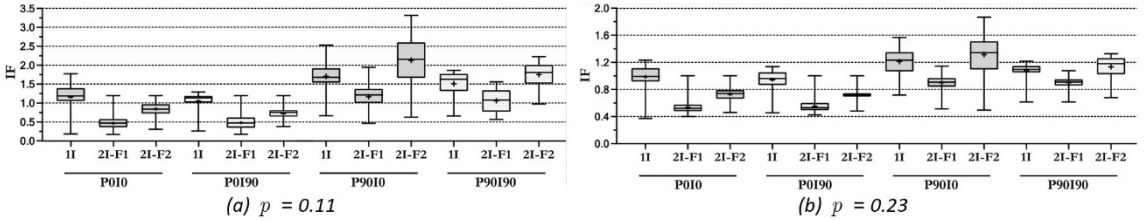


Figure 15 Variability of RMS torsion moment coefficients IFs

3.3 Power Spectra Density (PSD) of Aerodynamic Coefficients

The aerodynamic coefficients PSDs of the principal building were presented, analyzed with and without the interfering building in four positions, all of them with coordinate X = 6B and coordinate Y = 0B, 2B, 4B and 6B, enabling the analysis of oblique distances from the principal building. Cases with fixed interfering buildings (F1 and F2) were also analyzed. For a better comparison, the PSD was plotted normalized and as a function of the reduced frequency.

3.3.1 Along-wind Force PSD

Figures 16 and 17 present the along-wind force PSD at P0 (Fx) and P90 (Fy), respectively, varying the interfering buildings sets. At P0 it can be seen there is no occurrence of a sharp energy peak in the isolated case. However, when adding the I0 interfering buildings sets, Figures 16a to 16c, it is verified the existence of phenomenon with concentrated peaks of energy in most configurations, very close to the Strouhal number of the principal building $S_t = nD / \bar{U}_H \cong 0.1$ indicating that the vortex shedding frequency of interfering building coincides to the principal building one. The exception occurred in the presence of the upstream building in tandem position - (X; Y) = (6B; 0B) - where there was no energy peak in the 1I configuration. In 2I-F2 set there were two peaks, one at low frequency and another at high frequency. These peaks, outside the vortex shedding frequency, may have been generated by the buffeting effect, due to the variable interfering building distance, as seen in Blessmann (1985) and Gu et al. (2005), or by the Venturi effect (or a combination of both phenomena) since the fixed interfering building F2 was very close to the variable one, providing an accelerated approaching wind flow in the narrow passage between it.

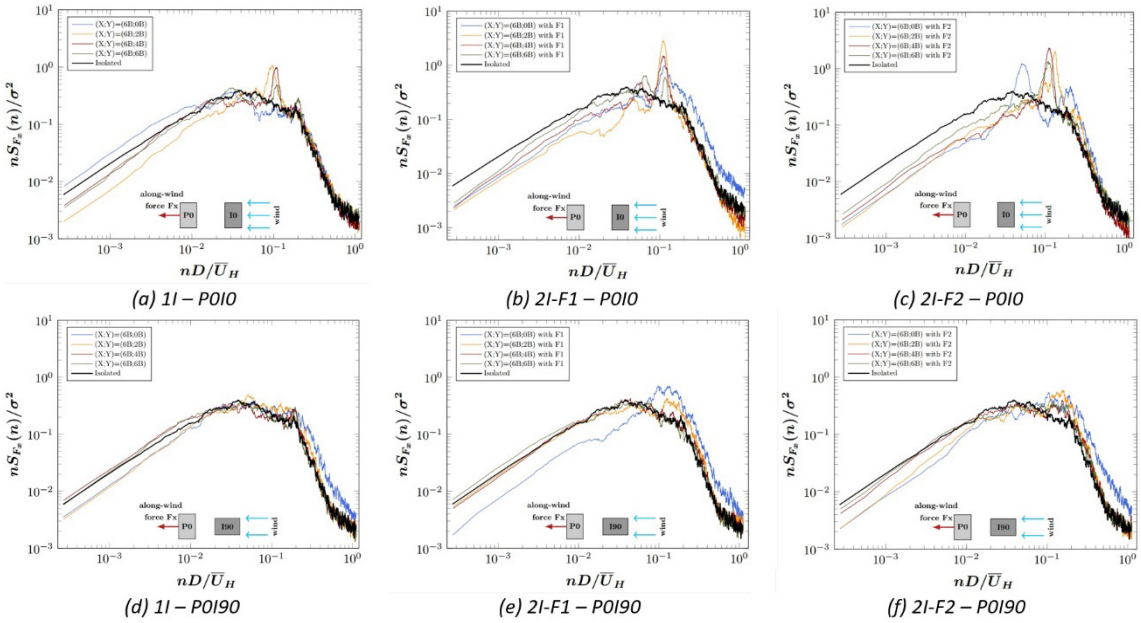


Figure 16 Along-wind force spectra for P0 and interference buildings (I0 and I90) at various distances

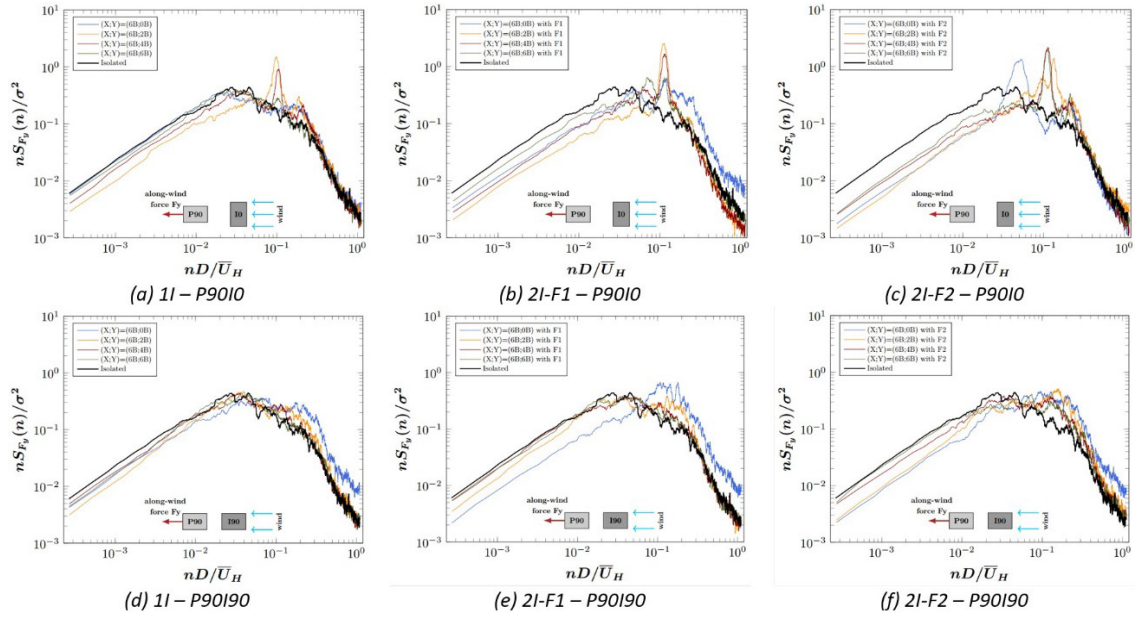


Figure 17 Along-wind force spectra for P90 and interference buildings (I0 and I90) at various distances

In the I90 interfering buildings sets, Figures 16d to 16f, it was verified the absence of energy peaks. What was observed are more energetic spectra in the presence of both fixed upstream buildings with the variable one at Y = 0B and 2B coordinates. A decrease in energy is observed as the variable interfering building is obliquely distanced from the principal building, exhibiting similar behavior to that of the 1I configuration, where all spectra had a similar appearance to the isolated building PSD.

The PSD behavior at P90, Figure 17, is quite similar to that observed at P0 for all the upstream buildings cases, that is, showing energy peaks in the presence of I0 sets with the potential to cause dynamic effects, nonexistent in the isolated case. It was seen that in I90 sets the spectra converge to the PSD shape of the isolated case, but with more energy at high frequencies, the closer the variable interfering building gets to tandem position.

3.3.2 Across-wind Force PSD

The Figures 18 and 19 present the across-wind force PSD at P0 (Fy) and P90 (Fx), respectively, varying the interfering buildings sets. At P0 it is possible to observe the occurrence of vortex shedding for the isolated case, with a sharp energy peak at frequency 0.1. With the interfering buildings I0 configuration, Figures 18a to 18c, all spectra in the 1I sets

presented a similar behavior to the isolated case, but with increased energy at higher frequencies for cases closer to the tandem position, so as observed by Zu and Lam (2018). When the fixed interfering building F1 is added, a second peak appears in the spectra, both in an attenuated form. However, these peaks are displaced, one to lower frequencies and the other to the vortex shedding frequency, suggesting the presence of an additional dynamic phenomenon. With the fixed interfering building F2, there is a tendency to the isolated peak in PSD, as the variable interfering building moves away from the tandem positions. With the interfering buildings I90 configuration, Figures 18d to 18f, the spectra did not show the double peak as in the I0 configuration, but with its peaks less attenuated compared to the last configuration, except for the variable interfering building in tandem position.

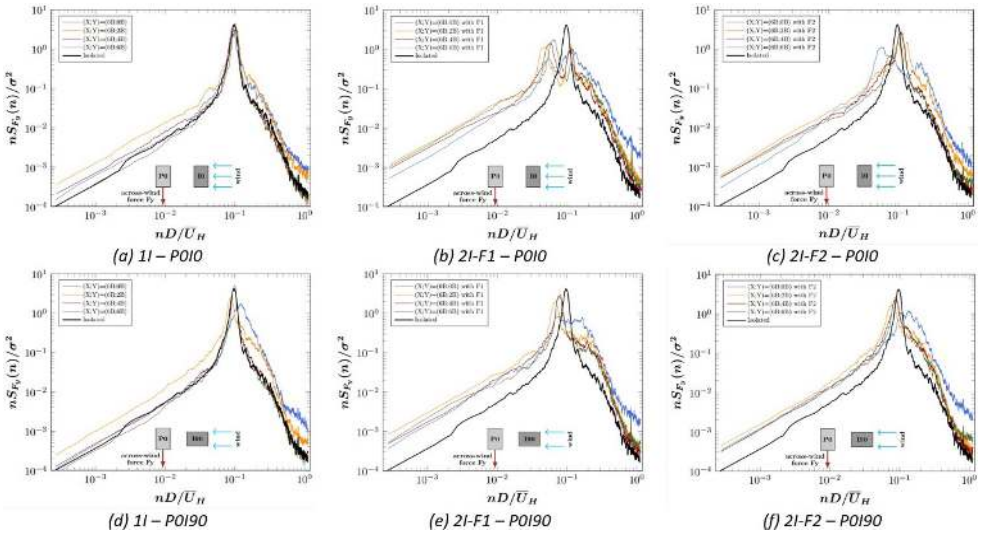


Figure 18 Across-wind force spectra for P0 and interference buildings (I0 and I90) at various distances

In the P90 configuration, there is a small mitigation of the energy peak at the vortex shedding frequency for the isolated case, relative to the peak of the P0 configuration. In the I0 interfering buildings configuration, Figures 19a to 19c, the spectra in the 1I sets presented amplifications in the energy peaks concentrated in the frequency 0.1, mitigated as the interfering building moves away from the tandem position. As in P0 configuration, in the 2I-F1 sets two peaks appeared in each PSD, again one for lower frequencies and the other at the vortex shedding frequency, but smoother. In the presence of fixed interfering building F2, which is more distanced from the principal building, the PSD shape of 1I sets was returned, except for the variable interfering building in tandem position, which still presented a double sharp peak, both offset from the 0.1 frequency.

In the I90 interfering buildings configuration, Figures 19d to 19f, the spectra of all interfering buildings cases presented a similar behavior to the isolated case.

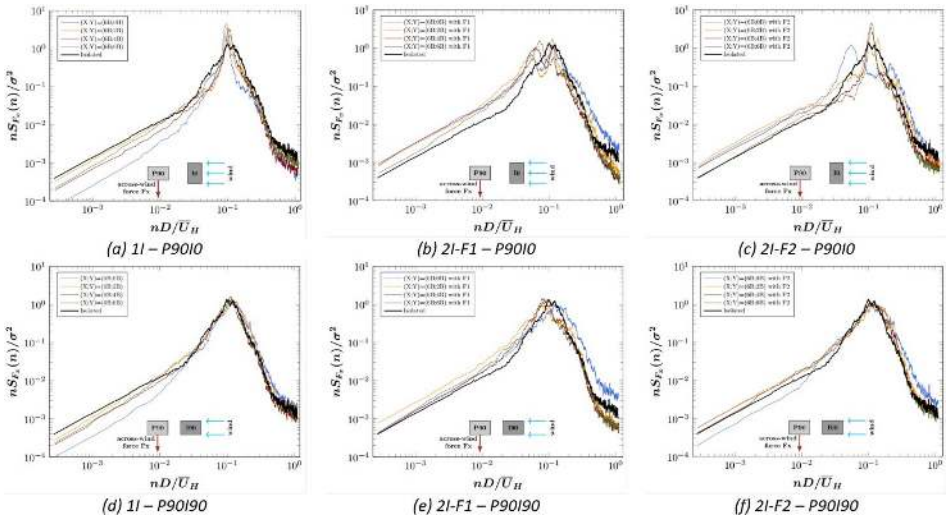


Figure 19 Across-wind force spectra for P90 and interference buildings (I0 and I90) at various distances

3.3.3 Torsional moment PSD

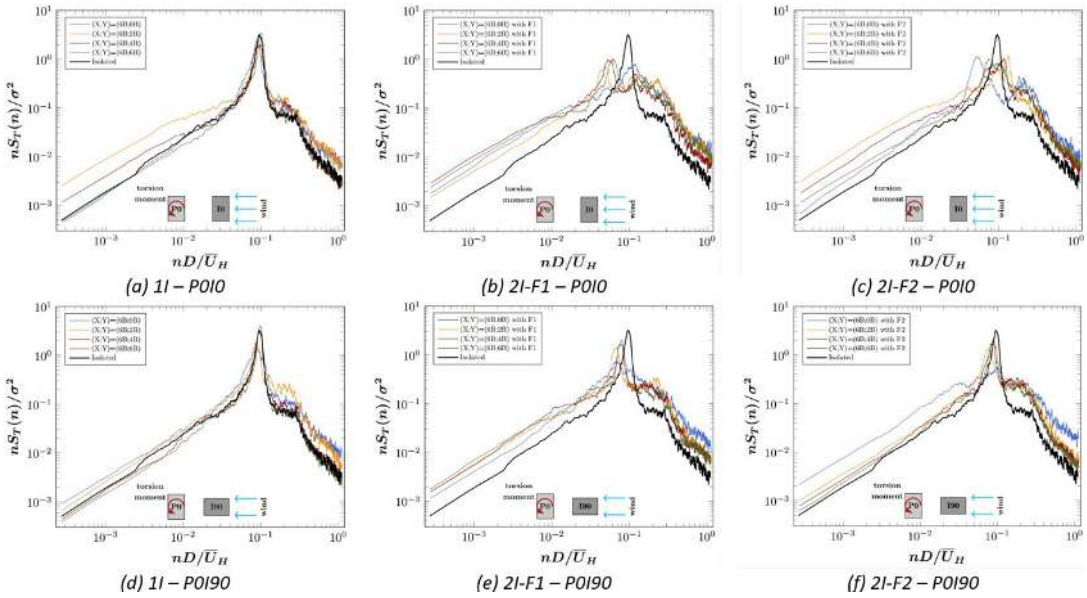


Figure 20 Torsion moment spectra for P0 and interference buildings (I0 and I90) at various distances

The Figures 20 and 21 present the torsional moment PSD at P0 and P90, respectively, varying the interfering buildings sets. In the P0 configurations, at both I0 and I90, the PSD shape with only one upstream building is very similar to that of the isolated case. When adding the fixed interfering buildings, both F1 and F2, there was attenuation and displacement of energy peaks in all cases, but in the rest of the frequency range there was an increase in the energy relative to the isolated case. In P90 configurations it is possible to notice that, for the isolated case, there is no evident PSD energy peak, that would indicate the vortex-induced resonance. In I0 interfering buildings configuration, Figures 21a to 21c, both for the 1I and 2I-F1 sets, there was the appearance of sharp peaks in the vortex shedding frequency with interfering buildings closer to the tandem position, but smoother in the presence of the fixed interfering building. In the 2I-F2 sets, there were energy peaks with more important amplifications the further away the interfering building was from the tandem position, being mitigated for the upstream building located in this position.

In I90 configurations, Figs. 21d to 21f, the spectra presented, in all interfering buildings cases, a similar behavior to the isolated case, with attenuation of the energy peak at the vortex shedding frequency.

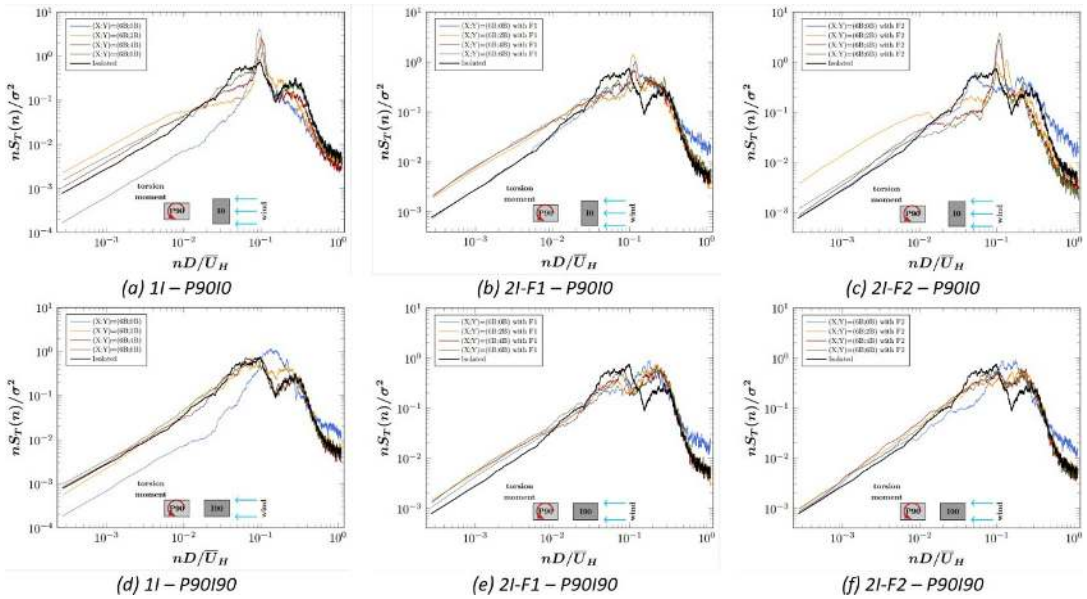


Figure 21 Torsion moment spectra for P90 and interference buildings (I0 and I90) at various distances

4 CONCLUSIONS

Interference effects were investigated by a series of wind tunnel tests, applying the synchronous pressure measurement technique in a rigid model. The influences of the distance and number of interfering buildings, angle of wind incidence, relative rotation of buildings and terrain roughness were evaluated. Based on the analysis of the experimental results, some conclusions can be summarized as follows:

1. From the contour plots of the interference factors (IFs) of the aerodynamic coefficients with roughness p = 0.23, it was observed that the greatest extension of the amplification zones occurred in the case when the incident wind was against to the smaller principal building façade (P90) and the larger interfering building facade (I0), that is, in the P90I0 sets. For the mean along-wind force coefficient, the fixed interfering buildings caused protection at P0 and amplifications at P90, mainly in the presence of F1 closer to the principal building. The same happened with the RMS across-wind force coefficient and RMS torsional moment, however, it was the F2 fixed interfering building, farthest from the principal building, which caused the higher amplification. The maximum IFs values of the RMS across-wind force coefficient occurred in the region (X/B; Y/B) = (3–6; 2–5).
2. The addition of turbulence in the approaching wind flow, that is, the change in wind profile from roughness exponent p = 0.11 to 0.23, was not enough to verify large alterations in the mean along-wind and RMS across-wind force coefficients on the building model, even presenting IFs with higher magnitudes on rougher terrain. The visible change occurred in the RMS torsional moment coefficient, where the low level of turbulence added to the smoother approaching flow generated significant reductions in the effects of upstream buildings interference.
3. Energy peaks in the PSD, indicating the possibility of vortex-induced resonance, were identified for along-wind force when interference buildings are rotated at 0° (P0I0 and P90I0 sets) and for the torsional moment in the P90I0 sets. In the across-wind force PSD, two energy peaks were identified in the P0I0 sets, in the presence of fixed interfering buildings. These sharp peaks were attenuated and displaced relative to the isolated building PSD peak, suggesting the action of the buffeting effect and/or Venturi effect.
4. The complexity of the phenomenon, so mentioned by previous studies and standards, was observed by the findings. However, the IFs in the arrangements with one interfering building are consistent with the values prescribed by Brazilian and Indian standards. Thus, it can be considered, in preliminary study of the structural designs, as a factor that increases wind loads on the isolated rectangular buildings, which must then be adjusted or determined by wind tunnel tests.
5. In general, for static analysis, the shielding effect in case of wind interference is a complex phenomenon and it is predominant in most of the studied cases. Nevertheless, the design parameters need to come from the amplification effects.

Author's Contributions: Conceptualization, Methodology and Writing - original draft, TFA de Lavôr; Writing - review & editing, JLV de Brito and AM Loredo-Souza; Supervision, AM Loredo-Souza.

Editor: Pablo Andrés Muñoz Rojas

References

ABNT NBR 6123 (1988), "Wind forces on buildings", Brazilian Association of Technical Standards; Rio de Janeiro, Brazil.

Barlow, B. J., Rae, W. H. Jr. and Pope, A. (1999), Low-speed Wind Tunnel Testing, 3th edition, John Wiley & Sons, New York, USA.

Blessmann, J. (1985), "Buffeting effects on neighbouring tall buildings", J. Wind Eng. Ind. Aerod., 18(1),105–110.

Gu, M., Xie, Z.N. and Huang, P. (2005), "Along-wind dynamic interference effects of tall buildings", Adv.Struct. Eng., 8(6), 623–636.

Fontes-Silva, P.H., Loredo-Souza, A.M. and Rocha, M.M. (2022), "Experimental study in wind tunnel of interference effects on the reduced model of the CAARC building." Latin American Journal of Solids and Structures 19(2), 1–13.

Hui, Y., Yoshida, A. and Tamura, Y. (2013), “Interference effects between two rectangular-section high-rise buildings on local peak pressure coefficients”, J. Fluids Struct., 37, 120–133.

Hui, Y., Tamura, Y. and Yang, Q. (2017), “Analysis of interference effects on torsional moment between two high-rise buildings based on pressure and flow field measurement”, J. Wind Eng. Ind. Aerod., 164, 54–68.

IS 875 (Part 3) (2015), “Design loads (other than earthquake) for buildings and structures–code of practice”, Bureau of Indian Standard; New Delhi, India.

Kim, W., Tamura, Y. and Yoshida, A. (2015), “Interference effects on aerodynamic wind forces between two buildings”, J. Wind Eng. Ind. Aerod., 147, 186–201.

Lo, Y.L., Li, Y.C. and Kim, Y.C. (2020), “Downstream interference effect of low-Scruton-number high-rise buildings under turbulent boundary layer flow”, J. Wind Eng. Ind. Aerod., 198, 104101.

Mara, T.G., Terry, B.K., Ho, T.C.E. and Isyumov, N. (2014), “Aerodynamic and peak response interference factors for an upstream square building of identical height”, J. Wind Eng. Ind. Aerod., 133, 200–210.

Pal, S., Meena, R.K., Raj, R., Anbukumar, S. (2021a), “Wind tunnel study of a fish-plan shape model under different isolated wind incidences”, Wind and Structures. 3(5), 353–366.

Pal, S., Raj, R., Anbukumar, S. (2021b), “Bilateral interference of wind loads induced on duplicate building models of various shapes”, Latin America Journal of Solids and Structures. 18(5), 1–17.

Taniike, Y. (1992), “Interference mechanism for enhanced wind forces on neighboring tall buildings”, J. Wind Eng. Ind. Aerod., 42(1-3), 1073–1083.

Vieira, G.S., Brito, J.L.V and Loredo-Souza, A.M. (2018), “Experimental study of the neighborhood effects on the mean wind loading over two equivalent high-rise buildings.” Latin American Journal of Solids and Structures 15(3), 1–15.

Xie, Z.N. and Gu, M. (2004), “Mean interference effects among tall buildings”, Eng. Struct., 26(9), 1173–1183.

Yu, X.F., Xie, Z.N., Wang, X. and Cai, B. (2016), “Interference effects between two high-rise buildings on wind-induced torsion”, J. Wind Eng. Ind. Aerod., 159, 123–133.

Zhang, W.J., Kwok, K.C.S. and Xu, Y.L. (1994), “Aeroelastic torsional behaviour of tall buildings in wakes”, J. Wind Eng. Ind. Aerod., 51(2), 229–248.

Zu, G.B. and Lam, K.M. (2018), “Across-wind excitation mechanism for interference of twin tall buildings in staggered arrangement”, J. Wind Eng. Ind. Aerod., 177, 167–185.